Atmos. Chem. Phys., 14, 13423–13437, 2014
www.atmos-chem-phys.net/14/13423/2014/
doi:10.5194/acp-14-13423-2014

Atmospheric Chemistry and Physics Open Access

Aerosol hygroscopicity and cloud condensation nuclei activity during the AC^{3}Exp campaign: implications for cloud condensation nuclei parameterization

F. Zhang[1], Y. Li[1], Z. Li[1,2], L. Sun[3], R. Li[1], C. Zhao[1], P. Wang[3], Y. Sun[4], X. Liu[5], J. Li[6,7], P. Li[6], G. Ren[6], and T. Fan[1]

[1]College of Global Change and Earth System Science, Beijing Normal University, 100875 Beijing, China
[2]Earth System Science Interdisciplinary Center and Department of Atmospheric and Oceanic Science, University of Maryland, College Park, Maryland, USA
[3]Key Laboratory of Middle Atmosphere and Global Environment Observation (LAGEO), Institute of Atmospheric Physics, Chinese Academy of Sciences, 100029 Beijing, China
[4]State Key Laboratory of Atmospheric Boundary Layer Physics and Atmospheric Chemistry, Institute of Atmospheric Physics, Chinese Academy of Sciences, 100029 Beijing, China
[5]State Key Laboratory of Water Environment Simulation, School of Environment, Beijing Normal University, 100875 Beijing, China
[6]Weather Modification Office of Shanxi Province, 030032 Taiyuan, China
[7]Key Laboratory for Aerosol-Cloud-Precipitation of China Meteorological Administration, Nanjing University of Information Science and Technology, 210044 Nanjing, China

Correspondence to: Z. Li (zli@atmos.umd.edu)

Received: 22 April 2014 – Published in Atmos. Chem. Phys. Discuss.: 6 June 2014
Revised: 24 October 2014 – Accepted: 10 November 2014 – Published: 16 December 2014

Abstract. Aerosol hygroscopicity and cloud condensation nuclei (CCN) activity under background conditions and during pollution events are investigated during the Aerosol-CCN-Cloud Closure Experiment (AC^{3}Exp) campaign conducted at Xianghe, China in summer 2013. A gradual increase in size-resolved activation ratio (AR) with particle diameter (D_p) suggests that aerosol particles have different hygroscopicities. During pollution events, the activation diameter (D_a) measured at low supersaturation (SS) was significantly increased compared to background conditions. An increase was not observed when SS was > 0.4 %. The hygroscopicity parameter (κ) was ∼ 0.31–0.38 for particles in accumulation mode under background conditions. This range in magnitude of κ was ∼ 20 %, higher than κ derived under polluted conditions. For particles in nucleation or Aitken mode, κ ranged from 0.20–0.34 for background and polluted cases. Larger particles were on average more hygroscopic than smaller particles. The situation was more complex for heavy pollution particles because of the diversity in particle composition and mixing state. A non-parallel observation CCN closure test showed that uncertainties in CCN number concentration estimates ranged from 30–40 %, which are associated with changes in particle composition as well as measurement uncertainties associated with bulk and size-resolved CCN methods. A case study showed that bulk CCN activation ratios increased as total condensation nuclei (CN) number concentrations (N_{CN}) increased on background days. The background case also showed that bulk AR correlated well with the hygroscopicity parameter calculated from chemical volume fractions. On the contrary, bulk AR decreased with increasing total N_{CN} during pollution events, but was closely related to the fraction of the total organic mass signal at m/z 44 (f_{44}), which is usually associated with the particle's organic oxidation level. Our study highlights the importance of chemical composition in determining particle activation properties and underlines the significance of long-term observations of CCN under different atmospheric environments, especially regions with heavy pollution.

Published by Copernicus Publications on behalf of the European Geosciences Union.

1 Introduction

The indirect influence of aerosol particles on the radiative balance of the atmosphere through changes in cloud droplet number and the persistence of clouds (Twomey, 1974; Albrecht, 1989) carries the largest uncertainty amongst the presently known causes of radiative forcing (IPCC, 2013). Thus, better understanding of aerosol particle formation, growth, and activation is essential.

Field and laboratory experiments have been conducted with the aim of better characterizing the particle physical and chemical parameters impacting on cloud condensation nuclei (CCN) activation. Studies have addressed the relative importance of the size distribution, particle composition, and mixing state in determining CCN activation, but there are disagreements on the relative importance of these parameters (e.g., Roberts et al., 2002; Feingold, 2003; Ervens et al., 2005; Mircea et al., 2005; Dusek et al., 2006a; Anttila and Kerminen, 2007; Hudson, 2007; Quinn et al., 2008; Zhang et al., 2008; Deng et al., 2013, Ma et al., 2013). CCN closure studies are a useful approach to test our knowledge of the controlling physical and chemical factors and to help verify experimental results. The CCN number concentration (N_{CCN}) is usually predicted from measured aerosol properties such as particle number size distribution and composition or hygroscopicity based on Köhler theory. The closure between the measured and estimated N_{CCN} is often achieved under background atmospheric conditions without heavy pollution (Chuang et al., 2000; Dusek et al., 2003; VanReken et al., 2003; Rissler et al., 2004; Gasparini et al., 2006; Stroud et al., 2007; Bougiatioti et al., 2009).

In urban and polluted areas, the particle size distribution is more complex (Lee et al., 2003; Alfarra et al., 2004; Zhang et al., 2004; Salcedo et al., 2006). Particle activation is affected by the composition and the mixing state of aerosol particles. It has been demonstrated that particles are more difficult to activate during biomass burning plume events (Mircea et al., 2005; Lee et al., 2006; Clarke et al., 2007; Rose et al., 2010, 2011; Paramonov et al., 2013; Lathem et al., 2013). Also, their activation ratios are reduced by secondary organics formed from oxidation of common biogenic emissions (VanReken et al., 2005; Varutbangkul et al., 2006; Mei et al., 2013) and black carbon (Dusek et al., 2006b; Kuwata et al., 2007). Other organic components (e.g., organic acids) have been shown to activate more easily (Raymond and Pandis, 2002; Hartz et al., 2006; Bougiatioti et al., 2011), but still much less than inorganic species. Therefore, testing the understanding of parameters controlling CCN activation and growth is challenging in heavily polluted areas. Furthermore, the main uncertainty in predicting the magnitude of global aerosol indirect effects arises from those regions under the influence of urban emissions (Sotiropoulou et al., 2007). The study of aerosol–CCN closure and relationships within, and in the outflow of, heavily polluted areas is thus important.

East Asia, especially the Jing (Beijing)–Jin (Tianjin)–Ji (Hebei) region, is a fast developing and densely populated region including numerous megacities, where anthropogenic aerosol emissions have increased significantly over recent years (Streets et al., 2008) and where aerosol loading is high and chemical composition is complex (Li et al., 2007a; Xin et al., 2007). The high aerosol loading significantly influences radiative properties, cloud microphysics, and precipitation (Xu, 2001; Li et al., 2007b; Xia et al., 2007; Rosenfeld et al., 2007; Lau et al., 2008; Li et al., 2011).

Field measurements of CCN have been made in East Asia, where megacities are likely to be major sources of pollutants and CCN (Yum et al., 2007; Rose et al., 2010, 2011; Gunthe et al., 2009; Yue et al., 2011; Liu et al., 2011; Zhang et al., 2012; Deng et al., 2011; Leng et al., 2013). Despite the significant accomplishments of these studies, limitations and uncertainties exist. As a recent example over the region of interest, Deng et al. (2011) over-predicted concentrations of CCN at a site in the North China Plain by 19 % compared with direct measurements.

The aim of this paper is to study aerosol hygroscopicity and CCN activity under high aerosol loading conditions and to parameterize CCN number concentrations by using CCN activation ratios (AR) as a proxy of the total number of aerosol particles in the atmosphere. A cumulative Gaussian distribution function (CDF) fit model is applied to aerosol data collected under clean and polluted conditions to examine the influence of size distribution, heterogeneity of chemical composition, and mixing state on CCN activity. The hygroscopicity parameter (κ) is derived using Köhler theory to study aerosol hygroscopicity on clean days and during pollution events. In the CCN closure study, in addition to the parallel observation (PO) closure test, we apply the CCN efficiency spectrum to non-simultaneous condensation nuclei (CN) and bulk CCN observations, namely the non-parallel observation (NPO) closure test, to estimate N_{CCN}. Finally, the relationship between bulk AR and aerosol physical and chemical properties is examined.

2 Measurements and data

An intensive field campaign called the Aerosol-CCN-Cloud Closure Experiment (AC^{3}Exp) was conducted during June and July of 2013 at the Xianghe Atmospheric Observatory (39.798° N, 116.958° E; 35 m a.s.l. (above sea level)) located about 60 km southeast of the Beijing metropolitan area. This site is surrounded by agricultural land, densely occupied residences, and light industry. Set between two megacities (Beijing to the northwest and Tianjin to the southeast) and less than 5 km west of the local town center (with a population of 50 000), the site experiences frequent pollution plumes. Depending on the wind direction, instruments at the Xianghe site detect pollutants of urban, rural, or mixed origins, experiencing both fresh biomass burning emissions and advected

aged aerosols. Details about the measurement location and meteorological conditions at the site can be found in Li et al. (2007b, 2011).

2.1 Instruments and measurements

Bulk CCN activation was measured from 1 to 25 June 2013. Size-resolved CCN were measured from 7 to 21 July 2013. Aerosol particle size distributions (10–700 nm) were measured from 1 to 25 June 2013 and from 7 to 21 July 2013. During 1–25 June 2013, a scanning mobility particle sizer (SMPS) was used independently for size distribution measurements. From 7 to 21 July 2013, it was combined with a Droplet Measurement Technologies-Cloud Condensation Nuclei Counter (DMT-CCNc) (Lance et al., 2006) and used for size-resolved CCN measurements. The CCN efficiency spectrum was derived from size-resolved CCN observations made from 7 to 21 July 2013. The aerosol particle size distribution data independently measured by the SMPS and bulk CCN measurements from 1 to 25 June 2013 combined with the derived CCN efficiency spectrum (Fig. 1) is used for the NPO CCN closure test. Aerosol chemical composition was measured from 31 May to 30 June 2013.

The aerosol inlet for the size distribution measurements was equipped with a TSI Environmental Sampling System (Model 3031200), which consists of a standard PM_{10} inlet, a sharp-cut PM_1 cyclone, and a bundled Nafion dryer. After drying, the sample flow with relative humidity (RH) of $< 30\,\%$ was drawn into the SMPS for the aerosol size distribution measurements (10–700 nm). Meanwhile, the bulk N_{CCN} at different supersaturation (SS) was measured, using a continuous-flow CCN counter from the DMT-CCNc. Each bulk CCN measurement cycle included three SS levels: 0.23, 0.51 and 0.80 %. The scanning times for those SS levels were set at 7, 5, and 5 min, respectively.

The size-resolved CCN efficiency spectra were measured by coupling the same DMT-CCNc used with the SMPS (Rose et al., 2008). In this setup the particles are rapidly dried with RH $< 30\,\%$ upon entering the Differential Mobility Analyzer (DMA). Thus, size selection is effectively performed under dry conditions, and the relative deviations in particle diameter should be $< 1\,\%$ except for potential kinetic limitations (Mikhailov et al., 2009). The sample flow exiting the DMA was split into two parts, with $0.3\,\mathrm{L\,min^{-1}}$ for the CPC and $0.5\,\mathrm{L\,min^{-1}}$ for the CCN_C. The DMA, controlled by the TSI-AIM software, scanned one size distribution every five minutes. The DMT-CCNc was operated at a total flow rate of $0.5\,\mathrm{L\,min^{-1}}$ with a sheath-to-aerosol flow ratio of 10. The inlet RH for DMT-CCNc was $< 30\,\%$. During the field campaign, the mean sample temperature and pressure measured by the DMT-CCNc sensors were $23.5 \pm 1.6\,^\circ\mathrm{C}$ and $985.5 \pm 3.6\,\mathrm{hPa}$. The SS levels of DMT-CCNc were calibrated with ammonium sulfate before and after the field campaign, following procedures outlined in Rose et al. (2008). During each CCN measurement cycle, calibrated effective

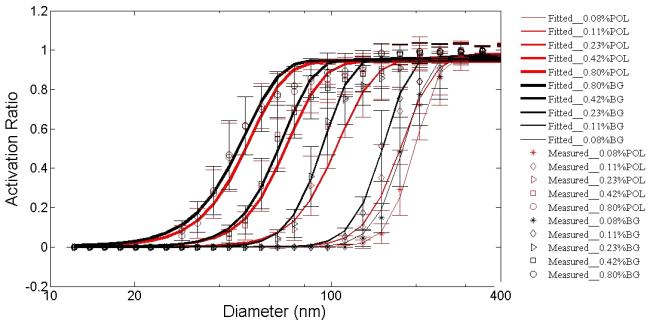

Figure 1. Averaged measured and fitted CCN efficiency spectra from the 3-parameter CDF fits at SS = 0.08, 0.11, 0.23, 0.42, and 0.80 % under polluted (POL) and background (BG) conditions during the size-resolved CCN measurement period.

SSs were 0.08, 0.11, 0.23, 0.42 and 0.80 %. The overall error (1σ) for the SS levels was estimated to be $< 3.5\,\%$. The completion of a full measurement cycle took 60 min (20 min for SS = 0.08 % and 10 min for the other SS levels).

The measurement of non-refractory submicron aerosol species including organics, sulfate, nitrate, ammonium, and chloride were made with an Aerodyne Aerosol Chemical Speciation Monitor (ACSM) (Sun et al., 2012). The ACSM uses the same aerosol sampling, vaporization and ionization modules as the Aerosol Mass Spectrometer (AMS) (DeCarlo et al., 2006), but removes the size components. During the field campaign, ambient aerosols were drawn inside through a 1/2 in. (outer diameter) stainless steel tube at a flow rate of $\sim 3\,\mathrm{L\,min^{-1}}$, of which $\sim 84\,\mathrm{cc\,min^{-1}}$ was subsampled into the ACSM. An URG cyclone (Model: URG-2000-30ED) was also supplied in front of the sampling inlet to remove coarse particles with a size cut-off of 2.5 mm. Before sampling into the ACSM, aerosol particles are dried by silica gel desiccant. The residence time in the sampling tube was $\sim 5\,\mathrm{s}$. The ACSM was operated at a time resolution of $\sim 15\,\mathrm{min}$ with a scan rate of the mass spectrometer of $500\,\mathrm{ms\,amu^{-1}}$ from m/z 10 to 150. Regarding the calibration of the ACSM, mono-dispersed, size-selected 300 nm ammonium nitrate particles within a range of concentrations were sampled into both the ACSM and a condensation particle counter (CPC). The ionization efficiency (IE) was then determined by comparing the response factors of the ACSM to the mass calculated with known particle size and number concentrations from the CPC. Once the IE was determined, changes in the internal standard naphthalene or air ions, e.g., m/z 28 (N_2^+) or m/z 32 (O_2^+), were used to account for the degradation of the detector. Other details including the instrument, aerosol sampling setup, operations, and calibration are given in Sun et al. (2012) and Ng et al. (2011).

In addition to the ACSM, the black carbon (BC) in $PM_{2.5}$ was simultaneously measured at a time resolution of 5 min by a BC analyzer (Aethalometer, Model AE22, Magee Scientific Corporation). The campaign averaged mass concentrations of BC were $\sim 4.2\,\mu g\,m^{-3}$, and the averaged mass fraction was about 6 %, with maximum of 18 % and minimum of 2 %. During the experiment period, the campaign area was generally hot and moist, with an average temperature of 23.6 °C and an average ambient RH of 72.3 %.

2.2 Data

The raw CCN data for both bulk and size-resolved CCN measurements were first filtered according to the instrument recorded parameters (e.g., temperature and flow). For example, if the relative difference between the actual and set sample flows was larger than 4 %, the data were flagged as invalid. If the "temperature stability" was recorded as "0", the data was also flagged as invalid data due to instrument fluctuations. These flagged data were not used for further analysis. A multiple charge correction and transfer function (Deng et al., 2011) was applied to each CN size distribution spectrum as well as to the CCN efficiency spectrum. The CCN AR is the ratio of N_{CCN} / N_{CN}. To examine CCN activity under different conditions, the size-resolved CCN efficiency data were classified as polluted or as background based on the aerosol loading as well as the synchronous surface horizontal wind data. Polluted conditions were identified when the total CN number concentration (N_{CN}) was $> 15\,000\,cm^{-3}$ and when the airflow came from the southeast or east. Background cases were identified when N_{CN} was $< 15\,000\,cm^{-3}$ and when winds were from the west or northwest. N_{CN} is the total aerosol number concentration with a particle size range of 10–700 nm. Here, the background refers to a regional background condition which represents a well-mixed atmosphere unaffected by local emissions, like biomass burning. Bulk measurements of total CCN number concentrations at SS levels of 0.23, 0.51 and 0.80 % could lead to a considerable underestimation of N_{CCN} under polluted conditions (Deng et al., 2011) due to water depletion inside the column (Lathem and Nenes, 2011). Therefore, in this study, data points with $N_{CN} > 25\,000\,cm^{-3}$ were excluded. In the closure study, CCN size distributions were calculated by multiplying the fitted campaign-averaged CCN efficiency spectrum (a 3-parameter CDF fit) with the aerosol particle number size distribution. The total N_{CCN} was then obtained by integrating the size-resolved N_{CCN} over the whole size range. Aerosol mass concentrations were processed using ACSM standard data analysis software (version 1.5.1.1). Detailed procedures for the data analysis have been described in Ng et al. (2011) and Sun et al. (2012).

3 Theory

As proposed by Petters and Kreidenweis (2007), κ can be used to describe the ability of particles to absorb water vapor and act as CCN. Based on Köhler theory (Köhler, 1936), κ relates the dry diameter of aerosol particles to the critical water vapor SS. According to measurements and thermodynamic models, κ is zero for insoluble materials like soot or mineral dust. However, their hygroscopicity changes due to the aging process, so the κ value then is > 0. The magnitude of κ is ~ 0.1 for secondary organic aerosols, ~ 0.6 for ammonium sulfate and nitrate, 0.95–1 for sea salt (Niedermeier et al., 2008), and 1.28 for sodium chloride aerosols. The effective hygroscopicity of mixed aerosols can be approximated by a linear combination of the κ values of the individual chemical components weighted by the volume or mass fractions (Kreidenweis et al., 2008; Gunthe et al., 2009). In this study, we calculated κ based on both size-resolved CCN measurements and bulk chemical composition observations made during the field campaign. The method to derive κ is described below.

3.1 Derivation of the average hygroscopicity parameter

The magnitude of κ was derived from the measured size-resolved CCN activated fraction using κ-Köhler theory (Petters and Kreidenweis, 2007). In κ-Köhler theory, the water vapor saturation ratio over an aqueous solution droplet, S_c, is given by:

$$S_c = \frac{D^3 - D_p^3}{D^3 - D_p^3(1-\kappa)} \exp\left(\frac{4\sigma_w M_w}{RT\rho_w D}\right), \quad (1)$$

where D is the droplet diameter, D_p is the dry diameter of the particle, M_w is the molecular weight of water, σ_w is the surface tension of pure water, ρ_w is the density of water, R is the gas constant, and T is the absolute temperature. When κ is greater than 0.1, it can be conveniently expressed as:

$$\kappa = \frac{4A^3}{27 D_p^3 S_c^2}, \quad (2)$$

where S_c is the particle critical supersaturation and is derived using the approach described by Rose et al. (2008), and A is defined as:

$$A = \frac{4\sigma_w M_w}{RT\rho_w D}. \quad (3)$$

The characteristic S_c of the size selected CCN is represented by the SS level at which AR reaches 50 %. For the parameters listed above, $T = 298.15\,K$, $R = 8.315\,J\,K^{-1}\,mol^{-1}$, $\rho_w = 997.1\,kg\,m^{-3}$, $M_w = 0.018015\,kg\,mol^{-1}$, and $\sigma_w = 0.072\,J\,m^{-2}$. Note that values derived from CCN measurement data through Köhler model calculations assume that the surface tension of pure water must be regarded as an "effective hygroscopicity parameter" accounting not

only for the reduction of water activity by the solute ("effective Raoult parameter") but also for surface tension effects (Petters and Kreidenweis, 2007). In this study, a parameter called κ_a, which characterizes the average hygroscopicity of CCN-active particles in the size range around activated diameters (D_a), is calculated from the data pairs of SS and D_a based on the κ-Köhler theory.

3.2 Derivation of the particle hygroscopicity

For a given internal mixture, κ can be predicted by a simple mixing rule on the basis of chemical volume fractions, ε_i (Petters and Kreidenweis, 2007; Gunthe et al., 2009):

$$\kappa_{chem} = \sum_i \varepsilon_i \kappa_i, \quad (4)$$

where κ_i and ε_i are the hygroscopicity parameter and volume fraction for the individual (dry) components in the mixture and i is the number of components in the mixture. We derive ε_i from the particle chemical composition measured by the ACSM. Measurements from the ACSM show that the composition of submicron particles was dominated by organics, followed by nitrate, ammonium, and sulfate. The contribution of chloride was negligible (with a volume fraction of about < 2 %). The analysis of the anion and cation balance suggests that anionic species (NO_3^-, SO_4^{2-}) were essentially neutralized by NH_4^+ over the relevant size range. For refractory species, BC represented a negligible fraction of the total submicron aerosol volume (less than 3 %). Sea salt and dust are usually coarse mode particles with particle sizes > 1 µm (Whitby, 1978). The contribution of such types of aerosols is thus expected to be negligible for sizes < 1000 nm. Therefore, the submicron particles measured by the ACSM mainly consisted of organics, $(NH_4)_2SO_4$, and NH_4NO_3. The particle hygroscopicity is thus the volume average of the three participating species:

$$\kappa_{chem} = \kappa_{Org}\varepsilon_{Org} + \kappa_{(NH_4)_2SO_4}\varepsilon_{(NH_4)_2SO_4} + \kappa_{NH_4NO_3}\varepsilon_{NH_4NO_3}. \quad (5)$$

The value of $\kappa_{(NH_4)_2SO_4}$ is 0.67 and $\kappa_{NH_4NO_3}$ is 0.61, derived from previous laboratory experiments (Petters and Kreidenweis, 2007). The following linear function derived by Mei et al. (2013) was used to estimate κ_{Org} in our study: $\kappa_{Org} = 2.10 \times f_{44} - 0.11$. The mean value of κ_{Org} during the field campaign wasps 0.115 ± 0.019. Species volume fractions were derived from mass concentrations and densities of participating species. The densities of $(NH_4)_2SO_4$ and NH_4NO_3 are 1770 kg m^{-3} and 1720 kg m^{-3}, respectively. The density of organics is 1200 kg m^{-3} (Turpin et al., 2001).

4 Results and discussion

4.1 Cumulative Gaussian distribution function fit and parameters derived from the cloud condensation nuclei efficiency

The spectra of measured CCN efficiency under both polluted and background conditions were fitted with a CDF (Rose et al., 2008):

$$f_{N_{CCN}/N_{CCN}} = a\left(1 + \mathrm{erf}\left(\frac{D - D_a}{\sigma_a\sqrt{2}}\right)\right), \quad (6)$$

where the maximum activated fraction (MAF) is equal to $2a$; D_a is the midpoint activation diameter; and σ_a is the CDF standard deviation. These parameters were determined for each spectrum. If MAF = 1 by changing the parameter "a" to 0.5, the spectrum is characteristic for internally mixed aerosols with homogeneous composition and hygroscopicity. The 3-parameter fit results represent the average activation properties of the aerosol particle fraction. During the field campaign, about 1200 size-resolved CCN efficiency spectra for atmospheric aerosols at SS levels of 0.08 to 0.80 % were measured. Figure 1 shows campaign-averaged spectra of both measured and fitted CCN efficiency at SS levels of 0.08, 0.11, 0.23, 0.42, and 0.80 % for background and polluted conditions. The slope of AR with respect to diameters near D_a in Fig. 1 provides information about the heterogeneity of the composition for the size-resolved particles. For an ideal case when all CCN-active particles have the same composition and size, a steep change of AR from 0 to MAF would be observed as D reaches D_a. A gradual increase in size-resolved AR with particle diameter suggests that aerosol particles consisted of different hygroscopicities. The gentler slopes of AR around D_a during pollution events show that the particle composition was more heterogeneous than the particle composition under background conditions. Significant differences in size-resolved CCN efficiency spectra under polluted and clean conditions at lower SS levels have been derived. The different shapes suggest that aerosol hygroscopicity and CCN activity would be affected by local emission sources, e.g., biomass burning.

4.1.1 Activation diameter

The three parameters (MAF, D_a, and σ), describing the CCN efficiency spectra derived from the 3-parameter CDF fits, and κ_a under polluted and clean conditions, are summarized in Table 1. Activation diameters under polluted and clean conditions are denoted as D_a_POL and D_a_BG in Table 1, respectively. As expected, D_a decreases with increasing SS under both background and polluted conditions. At a given SS, D_a_POL is greater than D_a_BG, suggesting that particles under polluted conditions would be activated at a larger diameter. As SS increases, the difference between D_a_POL and D_a_BG decreases.

Table 1. Parameters describing the CCN efficiency spectra and hygroscopicity for polluted (_POL) and background (_BG) cases: the activation diameter (D_a), the maximum activated fraction (MAF), the CDF standard deviation (σ), the heterogeneity parameter (σ/D_a), and the hygroscopicity parameter (κ_a) values shown are arithmetic mean values with one standard deviation averaged over the entire measurement period.

SS	D_a_POL	MAF_POL	σ_POL	σ/D_a_POL	κ_a_POL	D_a_BG	MAF_BG	σ_BG	σ/D_a_BG	κ_a_BG
0.08 %	190.43 ± 6.11	0.98 ± 0.01	33.34 ± 4.49	0.17 ± 0.02	0.32 ± 0.03	178.68 ± 4.22	0.98 ± 0.01	32.73 ± 2.07	0.18 ± 0.01	0.38 ± 0.02
0.11 %	161.80 ± 15.10	0.98 ± 0.01	38.61 ± 7.62	0.22 ± 0.03	0.26 ± 0.05	151.03 ± 2.90	0.97 ± 0.01	28.56 ± 1.97	0.19 ± 0.01	0.33 ± 0.02
0.23 %	94.05 ± 8.47	0.96 ± 0.01	27.87 ± 6.30	0.26 ± 0.04	0.31 ± 0.05	91.75 ± 2.48	0.96 ± 0.00	18.81 ± 1.53	0.20 ± 0.01	0.34 ± 0.02
0.42 %	63.33 ± 3.65	0.94 ± 0.01	18.02 ± 2.84	0.26 ± 0.03	0.30 ± 0.04	64.06 ± 1.24	0.95 ± 0.00	16.21 ± 0.81	0.25 ± 0.01	0.29 ± 0.01
0.80 %	44.78 ± 2.51	0.94 ± 0.01	14.08 ± 0.98	0.29 ± 0.01	0.24 ± 0.03	45.67 ± 1.29	0.95 ± 0.01	13.82 ± 1.17	0.30 ± 0.02	0.22 ± 0.02

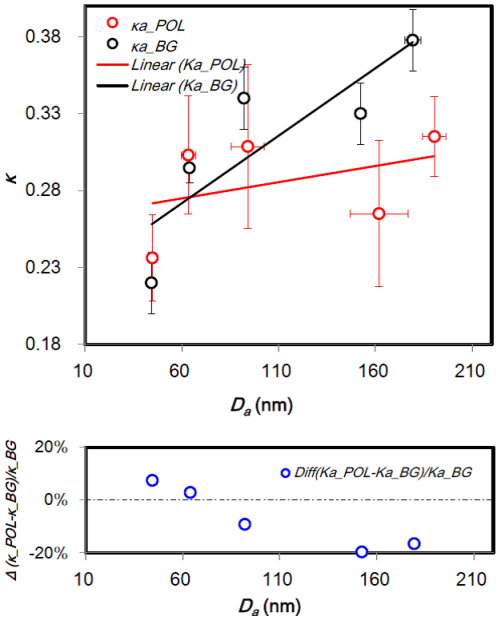

Figure 2. Derived hygroscopicity parameter, κ_a, as a function of particle diameter, D_a, under polluted (POL) and background (BG) conditions. Bottom: percent change in κ_a due to pollution as a function of D_a. Error bars represent one standard deviation calculated over the entire measurement period.

4.1.2 Maximum activated fraction

In general, aerosols with a more uniform and homogenous chemical composition or with a core-shell structure would have a higher MAF. The MAF under polluted and background conditions are denoted by MAF_POL and MAF_BG in Table 1. Values of MAF_BG and MAF_POL range from 0.95–0.98 and from 0.94–0.98, respectively. No significant discrepancies in MAF are observed between polluted and background conditions Observations show that particles can activate to CCN completely when particle diameters are greater than 300 nm even at SS = 0.08 %. This suggests that a smaller portion of 1− MAF (2–6 %) is caused by the error in the CDF fit, which will lead to a lower MAF than expected.

4.1.3 Cumulative Gaussian distribution function standard deviations

CDF standard deviations (σ) are general indicators for the extent of external mixing and the heterogeneity of particle composition for aerosols in the size range around D_a. CDF σ under polluted and background conditions are denoted as σ_POL and σ_BG in Table 1, respectively. Under ideal conditions, σ equals zero for an internally mixed, fully monodispersed aerosol with particles of homogeneous chemical composition. According to Rose et al. (2008), even after correcting for the DMA transfer function, calibration aerosols composed of high-purity ammonium sulfate exhibit small non-zero σ values that correspond to ∼ 3 % of D_a. This can be attributed to heterogeneities of the water vapor SS profile in the CCNc or other non-idealities, such as DMA transfer function and particle shape effects. Thus, "heterogeneity parameter" values of $\sigma/D_a = 3$ % indicate internally mixed CCN, whereas higher values indicate external mixtures of particles. Heterogeneity parameters under polluted and background conditions are denoted as σ/D_a_POL and σ/D_a_BG in Table 1, respectively. They range from 17–30 %, which is much higher than the 3 % observed for pure ammonium sulfate, indicating that the particles were externally mixed with respect to their solute content.

4.2 Derived average hygroscopicity parameter dependence on activation diameter

Figure 2 shows the dependence of κ_a on D_a under background and polluted conditions. κ_a_POL and κ_a_BG are defined as the average hygroscopicity of CCN-active particles in the size range around D_a under polluted and background conditions, respectively. For background days, larger particles were on average more hygroscopic than smaller particles, i.e., κ_a_BG increases substantially from about 0.22 at 30–60 nm to about 0.38 at a size range of 120–180 nm. This is consistent with field results observed in Guangzhou, South China by Rose et al. (2010). However, compared to κ_a_BG, κ_a_POL shows a relatively flat trend as the particle size diameter increases and error bars are larger. This suggests that under polluted conditions, particle composition and their mixing state is complex and diverse. In this case, larger particles

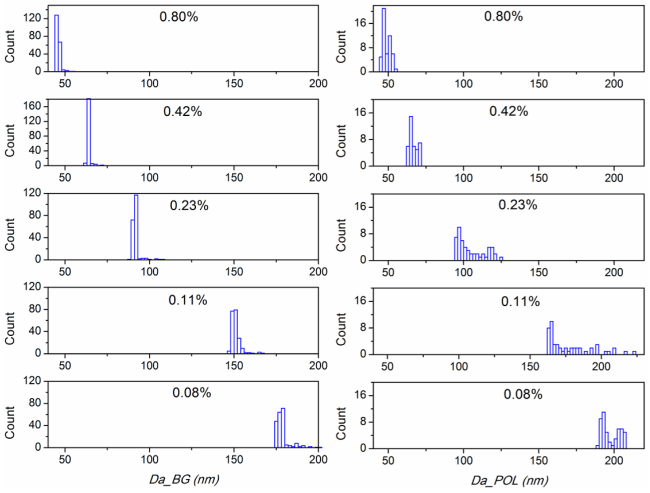

Figure 3. Probability distribution functions of D_a under background (_BG, left panels) and polluted (_POL, right panels) conditions at five SS levels (0.08–0.80 %) during the size-resolved CCN measurement period.

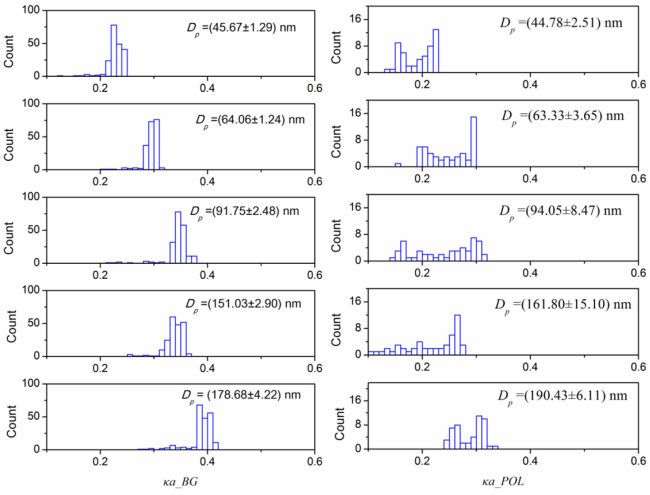

Figure 4. Probability distribution functions of κ_a under background (_BG, left panels) and polluted (_POL, right panels) conditions for different particle size ranges during the size-resolved CCN measurement period.

are even less hygroscopic than smaller particles. One possible reason for changes in κ_a under polluted conditions may be the presence of a high amount of organics freshly emitted from biomass burning (Andreae and Rosenfeld, 2008; Petters et al., 2009; Rose et al., 2010) which would coat the larger particles and render them less hygroscopic. Overall, κ for polluted aerosols is about 20 % lower than that for clean aerosol particles in the accumulation size range. For particles in the nucleation or Aitken size range, κ_a for polluted particles is slightly higher than that for particles in the background cases. Based on laboratory experiments, Petters et al. (2009) examined the hygroscopic properties of particles freshly emitted from biomass burning. They found that κ was a function of particle size, with 250 nm particles being generally weakly hygroscopic and sub-100 nm particles being more hygroscopic. During the field campaign, polluted cases occurred when particles were mainly biomass burning aerosols. The laboratory results, to some extent, can thus explain our field measurements. Further investigations, including laboratory experiments and field measurements of size-resolved chemical composition, are needed to confirm and clarify this.

4.3 Probability distribution functions of activation diameter and average hygroscopicity parameter

Figure 3 shows probability distribution functions (PDFs) for D_a under background conditions and during pollution events. D_a_POL are mainly distributed in the ranges of about 185–205, 163–180, 95–120, 65–75 and 45–55 nm at SS levels of 0.08, 0.11, 0.23, 0.42 and 0.80 %, respectively. At each SS level, the PDFs of D_a_POL have a wider distribution than the PDFs of D_a_BG. At each SS level, the PDFs of D_a_POL extend to large particle sizes indicating the impact by pollution. The largest variation in D_a_BG and D_a_POL is seen at SS = 0.08 % and 0.11 %, respectively. One reason for this is the weakened impact of chemical composition on CCN activity at high SS levels, i.e., the solute effect. The other reason is the larger uncertainties that arise from making measurements at low SS levels.

Figure 4 shows PDFs of κ_a under background conditions and during pollution events. The PDF of κ_a_POL has a large variation at each size range around D_p and shows two modes. For example, κ_a_POL for particles around 48 nm shows two peaks at ∼ 0.15 and ∼ 0.23. Peak values of ∼ 0.26 and ∼ 0.32 are seen for particles around D_p = 198 nm. Most κ_a_POL values are less than 0.3. This suggests externally mixed, but less hygroscopic particles are prevalent during pollution events. Less variation is seen in the PDFs of κ_a_BG. One mode is seen with peak values of 0.23, 0.30, 0.35, 0.35, and 0.38 for D_p = 46, 64, 92, 152, and 179 nm, respectively. Most κ_a_BG values are greater than 0.3 when D_p > 60 nm, indicating that the particles are more hygroscopic with a relatively homogeneous composition.

4.4 Cloud condensation nuclei closure tests

In this section, we compare observed total N_{CCN} with corresponding values that were estimated on the basis of aerosol particle number size distributions measured both in parallel and not in parallel and assuming a uniform particle composition. Closure was achieved when estimated and observed N_{CCN} agreed quantitatively within the range of their uncertainties.

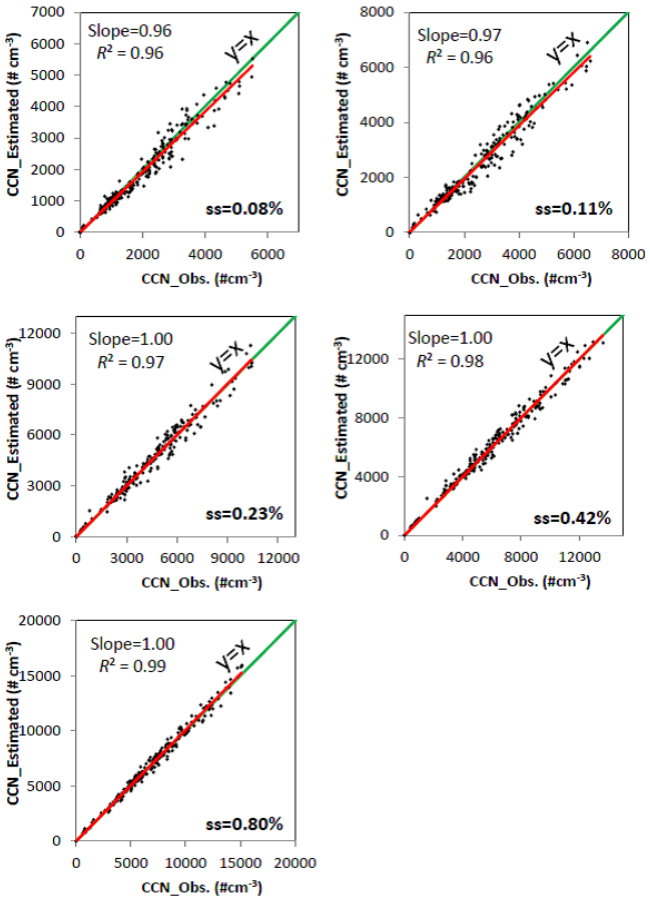

Figure 5. Estimated N_{CCN} as a function of observed N_{CCN} at different SS levels in the parallel observation (PO) closure test. The green solid line is the 1:1 line.

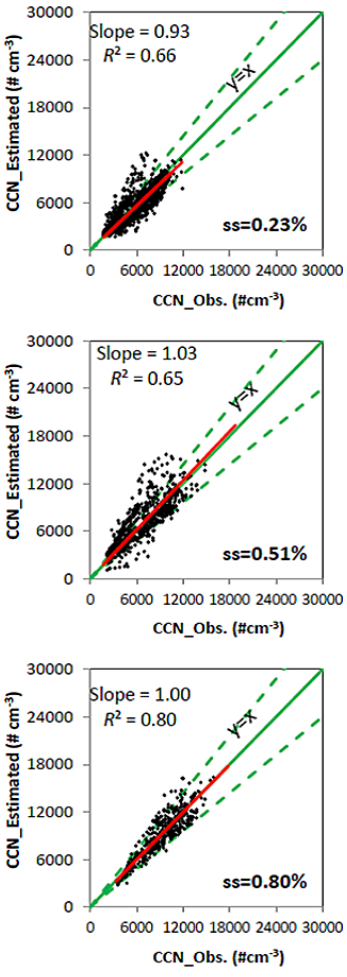

Figure 6. As in Fig. 5, but for the non-parallel observation (NPO) closure test. The dashed green lines indicate the boundaries representing ±30 % deviations of N_{CCN}-estimated from N_{CCN}-observed.

4.4.1 Parallel observation closure test

In parallel observation (PO) closure tests, the measured CCN efficiency spectrum is first multiplied by the measured CN size distribution, which yields the CCN size distribution. This is then integrated over the whole size range to obtain the observed total CCN concentration (CCN_Obs). Size-resolved N_{CCN} are calculated by multiplying the campaign-averaged CCN efficiency spectrum with simultaneously measured CN number size distributions. Estimated total N_{CCN} (CCN_Estimated) are obtained by the stepwise integration of size-resolved N_{CCN} from 10 to 700 nm. With this comparison, the influence of the variation in chemical composition on the CCN concentration can be investigated because the CN size distribution is the same for both parameters.

Figure 5 shows CCN_Estimated as a function of CCN_Obs at SS levels ranging from 0.08 to 0.80 %. Estimated and measured total N_{CCN} agree well. The mean slope and correlation coefficient (R^2) are 0.99 and 0.97, respectively, at the five SS levels. A ∼3–4 % underestimation occurs at SS levels of 0.08 and 0.11 %. One reason for this slight underestimation is that size-resolved ARs are more variable at low SS levels than at higher SS levels. Also, compared to total activated CCN number concentrations at high SS levels, there are fewer N_{CCN} at low SS levels, leading to larger uncertainties or to a lower correlation. Overall, CCN closure can be achieved by using campaign-averaged CCN efficiency spectra. In this PO closure test, the influence of variations in chemical composition on CCN concentrations is insignificant.

4.4.2 Non-parallel observation closure test

Mean CCN efficiency spectra derived from size-resolved CCN measurements taken on 7–21 July 2013 are used to estimate total CCN number concentrations based on CN size distribution measurements taken on 1–25 June 2013. This is referred to as a non-parallel observation (NPO) closure test. The average measured CCN efficiency spectrum (cor-

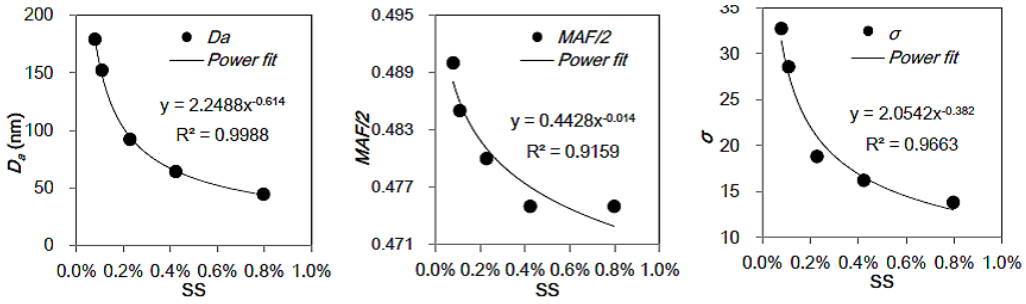

Figure 7. Activation diameter, D_a, maximum activated fraction, MAF, and standard deviation, σ, as a function of super saturation, SS.

responding to spectra in Fig. 1) is multiplied by the measured CN size distribution which yields the CCN size distribution. This is integrated over the whole size range (10–700 nm) to obtain the estimated total CCN concentration. The mean CCN efficiency spectra at SS levels of 0.23 and 0.80 % (Fig. 1) is used to estimate the total CCN concentration during 1–25 June 2013. The mean CCN efficiency spectra at SS = 0.51 % is derived using the exponential relationships developed from plotting the three CDF fit parameters as a function of SS (see Fig. 7).

Estimated total N_{CCN} as a function of measured bulk N_{CCN} at SS levels of 0.23, 0.51, and 0.80 % are shown in Fig. 6. The lower slope at SS = 0.23 % indicates that the estimation on the basis of NPO closure underestimates about 7 % of the observed N_{CCN}. The closure is considerably improved at higher SS levels. A reasonable correlation between estimated and measured total N_{CCN} is seen ($R^2 = 0.6 - 0.8$), which suggests temporal variations in chemical composition and mixing state of aerosol particles. In addition, there are uncertainties due to measuring bulk and size-resolved CCN. Overall, uncertainties in this NPO CCN closure study range from 30–40 %. Caution is needed when using data from any short-term experiment at a single site to do CCN parameterizations for large-scale applications. It is necessary to conduct long-term CCN measurements at more regional sites, especially those that are heavily polluted.

4.5 Case study: cloud condensation nuclei activation and chemical composition

The behavior of CCN activation under background and polluted conditions is examined. Two cases are selected: one case with total $N_{CN} < 15\,000$ cm^{-3} (background) and another case with total $N_{CN} > 15\,000$ cm^{-3} (polluted). Trends in bulk CCN activation as N_{CN} increases are different for the background and polluted cases. Bulk AR at the three SS levels (0.23, 0.51, and 0.80 %) increases as total N_{CN} increases for background cases (Fig. 8a) and decreases as total N_{CN} increases for polluted cases (Fig. 8b). For the background cases, changes in bulk AR are dependent on changes in κ_{chem} (Fig. 8c). A good correlation between AR_ 0.23 and κ_{chem} ($R^2 > 0.7$) is seen in Fig. 9. A high correlation between bulk AR and κ_{chem}, when total N_{CN} is low, is observed during the campaign (Fig. 10). In these cases, organics account for ~ 30 % of the total particle mass concentration and concentrations of soluble inorganics are high (Fig. 8e). In particular, the mass concentration of nitrate is higher than that for organics and accounts for the largest mass fraction when κ_{chem} reaches a maximum with a mean value of ~ 0.45. The f_{44}, which is the fraction of total organic mass signal at m/z 44, is not correlated with AR (Fig. 8c). The m/z 44 signal is mostly due to acids (Takegawa et al., 2007; Duplissy et al., 2011) or acid-derived species, such as esters, and f_{44} is closely related to the organic oxidation level, i.e., O : C ratio (Aiken et al., 2008). Oxidized/aged acids are generally more hygroscopic and easily activated. Therefore, the lower correlation between f_{44} and AR implies that organics under low N_{CN} conditions are less hygroscopic. CN number concentrations in the nucleation, Aitken, and accumulation modes are shown in Fig. 8g (polluted) and Fig. 8h (background). Under background conditions, bulk AR at SS = 0.23 % is more correlated ($R^2 = 0.5$) with changes in N_{CN} in the accumulation mode (Fig. 9), suggesting that most aerosol particles with sizes > 100 nm can be activated. Smaller particles with Aitken diameters of < 40 nm at the given SS levels (0.23–0.80 %) are not as easily activated, if at all, so no correlation is seen (Fig. 8g).

Under polluted conditions, there is little dependence of changes in bulk AR with changes in κ_{chem}(Fig. 8d). Bulk AR at SS = 0.23 % is moderately correlated with f_{44} ($R^2 = 0.5$, Fig. 9). As stated above, f_{44} is always related to the organic oxidation level. Usually, oxidized/aged acids are more hygroscopic and easily activated. The correlation between f_{44} and bulk AR suggests that the organics contribution from oxidized or aged aerosols play a significant role in CCN activity (Jimenez et al., 2009). A bias is introduced by using a parameterized function derived from observations made at other sites with different aerosol types to describe the particle hygroscopicity and activation properties due to the complexity of the organic aerosol fraction and its tendency to evolve with atmospheric oxidative processing and aerosol aging (e.g., Padró et al., 2010; Engelhart et al., 2011, 2012; Asa-Awuku et al., 2011). Under polluted conditions, the bulk AR_0.2 is

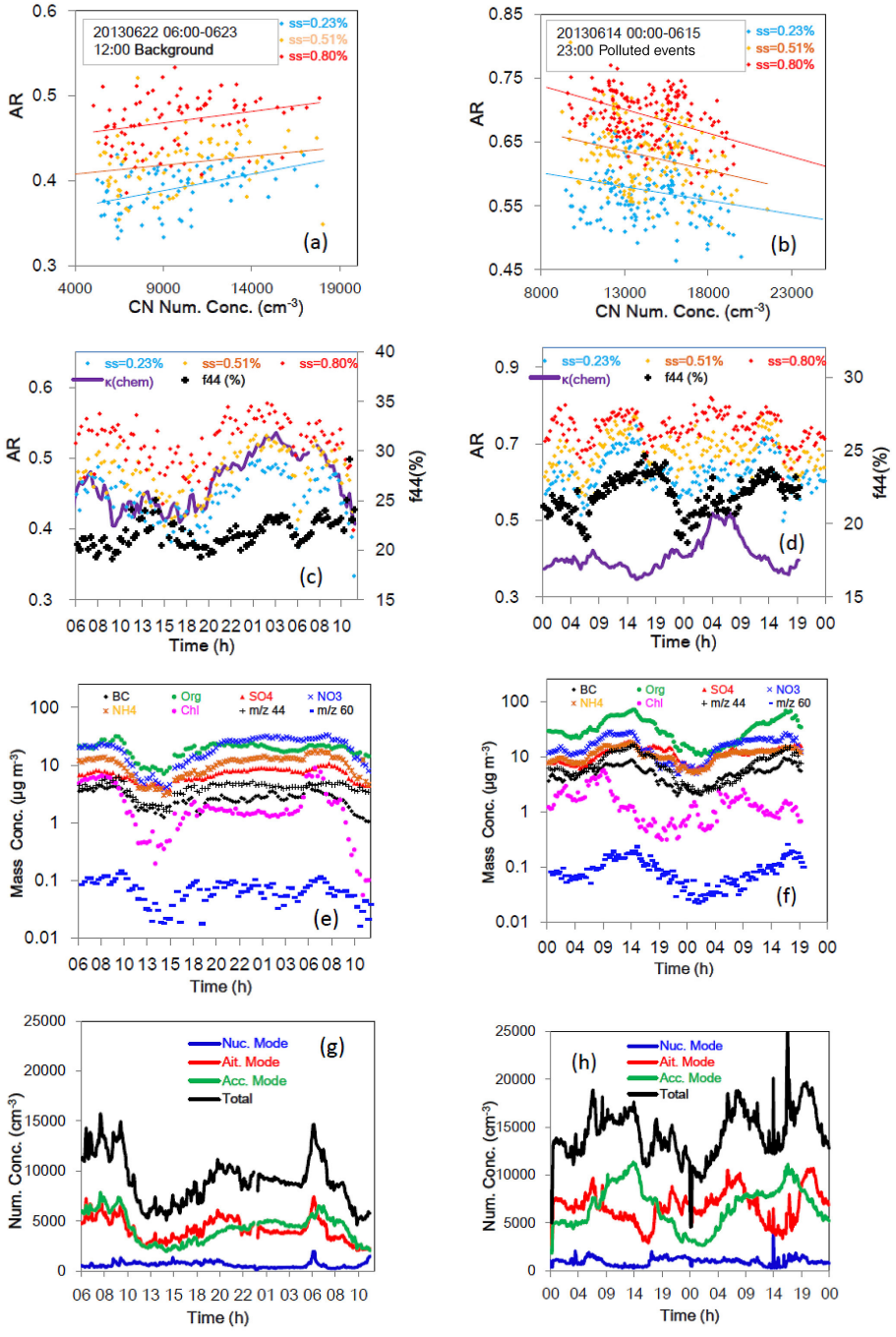

Figure 8. Measurements made under background conditions (22–23 June 2013, $N_{CN} < 15\,000\,cm^{-3}$) and polluted conditions (14–15 June 2013, $N_{CN} > 15\,000\,cm^{-3}$). Bulk CCN activation ratios at SS = 0.2, 0.5, and 0.8 % as a function of N_{CN} under background and polluted conditions are shown in **(a)** and **(b)**, respectively. Diurnal variations in AR, derived from κ_{chem} and the fraction of total organic mass signal at f_{44}, under background and polluted conditions are shown in **(c)** and **(d)**, respectively. Mass concentrations of black carbon (BC), organics, nitrate (NO_3^-), ammonium (NH_4^+), sulfate (SO_4^{2-}), chloride (Cl^-) ions, etc., under background and polluted conditions are shown in **(e)** and **(f)**, respectively. N_{CN} for nucleation (10–30 nm), Aitken (30–130 nm), and accumulation modes (130–700 nm) under background and polluted conditions are shown in **(g)** and **(h)**, respectively.

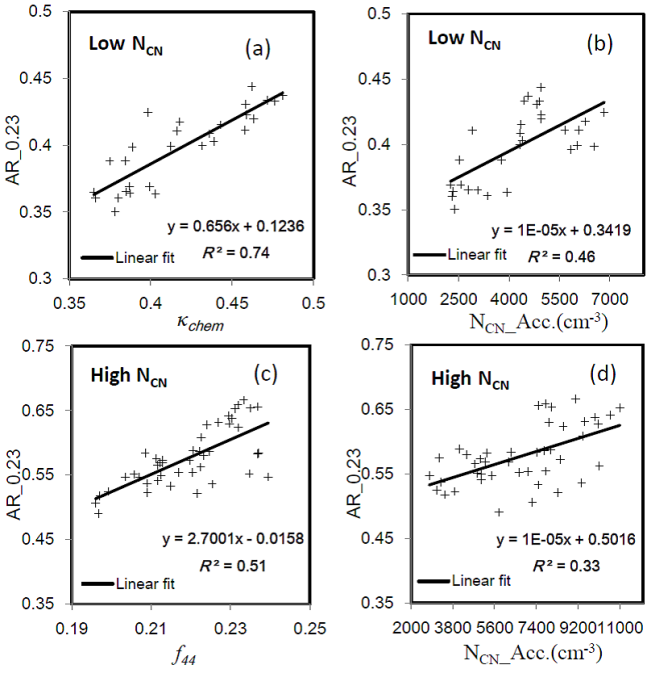

Figure 9. AR measured at SS = 0.23 % as a function of **(a)** κ_{chem} under background conditions, **(b)** accumulation mode N_{CN} under background conditions, **(c)** f_{44} under polluted conditions, and **(d)** accumulation mode N_{CN} under polluted conditions. The accumulation mode size range is 130–700 nm in this study.

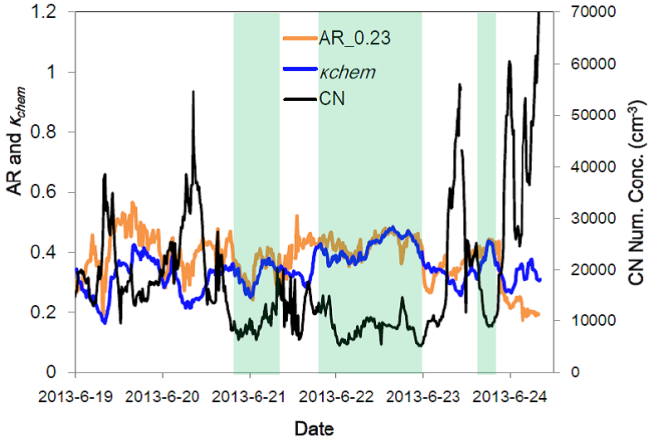

Figure 10. Time series of bulk AR at SS = 0.23 %, derived κ_{chem}, and N_{CN} from 19–24 June 2013. Green shaded areas highlight periods with high correlations between bulk AR and κ_{chem}.

more correlated with changes in accumulation mode particles ($R^2 = \sim 0.3$).

Overall, based on the case study, one cannot use a parameterized formula using only total N_{CN} to estimate total CCN number concentrations. If observations such as size-resolved CCN and size-resolved chemical composition are not available, the possibility of using bulk κ_{chem} and f_{44} in combination with bulk $N_{\mathrm{CN}} > 100$ nm to parameterize CCN number concentrations is implied by the case study. Further field investigations are needed to demonstrate and confirm the relationship between bulk AR and particle size and composition.

5 Summary and conclusions

Atmospheric aerosol particles acting as CCN are pivotal elements of the hydrological cycle and climate change. In this study, we measured and characterized N_{CCN} in relatively clean and polluted air during the AC^{3}Exp campaign conducted at Xianghe, China during summer 2013. The aim was to examine CCN activation properties under high aerosol loading conditions in a polluted region and to assess the impacts of particle size and chemical composition on the CCN AR, which acts as a proxy of the total number of aerosol particles in the atmosphere. Based on the CDF fit method, a gradual increase in size-resolved AR with particle diameter suggests that aerosol particles have different hygroscopicities. D_{a} increased significantly at lower SS levels (< 0.23 %) due to pollution, e.g., biomass burnings. This increase was not observed when SS > 0.4 %. For particles in the accumulation mode, values of κ ranged from 0.31–0.38 under background conditions, about 20 % higher than that derived under polluted conditions. For particles in the nucleation or Aitken mode, κ ranged from 0.20–0.34 under both background and polluted conditions. Larger particles were on average more hygroscopic than smaller particles. However, the case of particles originating from heavy pollution is more complex, due to the diversity in particle composition and mixing state. The low R^2 for the NPO CCN closure test suggests a 30–40 % uncertainty in total N_{CCN} estimation. Using bulk chemical composition data from ACSM measurements, the relationship between bulk AR and the physical and chemical properties of atmospheric aerosols is investigated. Based on a case study, we conclude that one cannot use a parameterized formula using only total N_{CN} to estimate total N_{CCN}. We have shown the possibility of using bulk κ_{chem} and f_{44} in combination with bulk $N_{\mathrm{CN}} > 100$ nm to parameterize CCN number concentrations. Further field investigations or examinations are needed to demonstrate and confirm the relationship between bulk AR and particle size and composition.

Acknowledgements. We thank the reviewers for their suggestions and comments which have greatly improved the paper. This work was funded by the National Basic Research Program of China "973" (grant nos. 2013CB955801, 2013CB955804), the National Science Foundation (grant no. 1118325), the Fundamental Research Funds for the Central Universities (grant no. 2013YB35) and the National Natural Science Foundation of China (NSFC) and Texas A & M University Research Grant Program (grant no. 41411120223). We greatly appreciate the support of the entire AC^{3}Exp team.

Edited by: J. Allan

References

Aiken, A. C., DeCarlo, P. F., Kroll, J. H., Worsnop, D. R., Huffman, J. A., Docherty, K. S., Ulbrich, I. M., Mohr, C., Kimmel, J. R., Sueper, D., Sun, Y., Zhang, Q., Trimborn, A., Northway, M., Ziemann, P. J., Canagaratna, M. R., Onasch, T. B., Alfarra, M. R., Prevot, A. S. H., Dommen, J., Duplissy, J., Metzger, A., Baltensperger, U., and Jimenez, J. L.: O/C and OM/OC ratios of primary, secondary, and ambient organic aerosols with high-resolution time-of-flight aerosol mass spectrometry, Environ. Sci. Technol., 42, 4478–4485, 2008.

Albrecht, B. A.: Aerosols, clouds and microphysics, Science, 245, 1227–1230, 1989.

Alfarra, M. R., Coe, H., Allan, J. D., Bower, K. N., Boudries, H., Canagaratna, M. R., Jimenez, J. L., Jayne, J. T., Garforth, A. A., Li, S.-M., and Worsnop, D. R.: Characterization of urban and rural organic particulate in the Lower Fraser Valley using two Aerodyne Aerosol Mass Spectrometers., Atmos. Environ., 38, 5745–5758, 2004.

Andreae, M. O. and Rosenfeld, D.: Aerosol-cloud precipitation interactions. Part 1. The nature and sources of cloud-active aerosols, Earth. Sci. Rev., 89, 13–41, doi:10.1016/j.earscirev.2008.03.001, 2008.

Anttila, T. and Kerminen, V.-M.: On the contribution of Aitken mode particles to cloud droplet populations at continental background areas – a parametric sensitivity study, Atmos. Chem. Phys., 7, 4625–4637, doi:10.5194/acp-7-4625-2007, 2007.

Asa-Awuku, A., Moore, R. H., Nenes, A., Bahreini, R., Holloway, J. S., Brock, C. A., Middlebrook, A. M., Ryerson, T., Jimenez, J., DeCarlo, P., Hecobian, A., Weber, R., Stickel, R., Tanner, D. J., and Huey, L. G.: Airborne cloud condensation nuclei measurements during the 2006 Texas Air Quality Study, J. Geophys. Res., 116, D11201, doi:10.1029/2010JD014874, 2011.

Bougiatioti, A., Fountoukis, C., Kalivitis, N., Pandis, S. N., Nenes, A., and Mihalopoulos, N.: Cloud condensation nuclei measurements in the marine boundary layer of the Eastern Mediterranean: CCN closure and droplet growth kinetics, Atmos. Chem. Phys., 9, 7053–7066, doi:10.5194/acp-9-7053-2009, 2009.

Bougiatioti, A., Nenes, A., Fountoukis, C., Kalivitis, N., Pandis, S. N., and Mihalopoulos, N.: Size-resolved CCN distributions and activation kinetics of aged continental and marine aerosol, Atmos. Chem. Phys., 11, 8791–8808, doi:10.5194/acp-11-8791-2011, 2011.

Chuang, P. Y., Collins, D. R., Pawlowska, H., Snider, J. R., Jonsson, H. H., Brenguier, J. L., Flagan, R. C., and Seinfeld, J. H.: CCN measurements during ACE-2 and their relationship to cloud microphysical properties, Tellus B, 52, 843–867, 2000.

Clarke, A., McNaughton, C., Kasputin, V. N., Shinozuka, Y., Howell, S., Dibb, J., Zhou, J., Anderson, B., Brekhovskikh, V., Turner, H., and Pinkerton, M.: Biomass burning and pollution aerosol over North America: Organic components and their influence on spectral optical properties and humidification response, J. Geophys. Res., 112, D12S18, doi:10.1029/2006JD007777, 2007.

DeCarlo, P. F., Kimmel, J. R., Trimborn, A., Northway, M. J., Jayne, J. T., Aiken, A. C.,Gonin, M., Fuhrer, K., Horvath, T., Docherty, K. S., Worsnop, D. R., and Jimenez, J. L.: Field-deployable, high-resolution, time-of-flight aerosol mass spectrometer, Anal. Chem., 78, 8281–8289, 2006.

Deng, Z. Z., Zhao, C. S., Ma, N., Liu, P. F., Ran, L., Xu, W. Y., Chen, J., Liang, Z., Liang, S., Huang, M. Y., Ma, X. C., Zhang, Q., Quan, J. N., Yan, P., Henning, S., Mildenberger, K., Sommerhage, E., Schäfer, M., Stratmann, F., and Wiedensohler, A.: Size-resolved and bulk activation properties of aerosols in the North China Plain, Atmos. Chem. Phys., 11, 3835–3846, doi:10.5194/acp-11-3835-2011, 2011.

Deng, Z. Z., Zhao, C. S., Ma, N., Ran, L., Zhou, G. Q., Lu, D. R., and Zhou, X. J.: An examination of parameterizations for the CCN number concentration based on in situ measurements of aerosol activation properties in the North China Plain, Atmos. Chem. Phys., 13, 6227–6237, doi:10.5194/acp-13-6227-2013, 2013.

Dusek, U., Covert, D. S., Wiedensohler, A., Neususs, C., Weise, D., and Cantrell, W.: Cloud condensation nuclei spectra derived from size distributions and hygroscopic properties of the aerosol in coastal south-west Portugal during ACE-2, Tellus B, 55, 35–53, 2003.

Dusek, U., Frank, G. P., Hildebrandt, L., Curtius, J., Schneider, J., Walter, S., Chand, D., Drewnick, F., Hings, S., Jung, D., Borrmann, S., and Andreae, M. O.: Size matters more than chemistry for cloud-nucleating ability of aerosol particles, Science, 312, 1375–1378, 2006a.

Dusek, U., Reischl, G. P., and Hitzenberger, R.: CCN activation of pure and coated carbon black particles, Environ. Sci. Technol., 40, 1223–1230, 2006b.

Duplissy, J., DeCarlo, P. F., Dommen, J., Alfarra, M. R., Metzger, A., Barmpadimos, I., Prevot, A. S. H., Weingartner, E., Tritscher, T., Gysel, M., Aiken, A. C., Jimenez, J. L., Canagaratna, M. R., Worsnop, D. R., Collins, D. R., Tomlinson, J., and Baltensperger, U.: Relating hygroscopicity and composition of organic aerosol particulate matter, Atmos. Chem. Phys., 11, 1155–1165, doi:10.5194/acp-11-1155-2011, 2011.

Engelhart, G. J., Moore, R. H., Nenes, A., and Pandis, S. N.: Cloud condensation nuclei activity of isoprene secondary organic aerosol, J. Geophys. Res., 116, D02207, doi:10.1029/2010JD014706, 2011.

Engelhart, G. J., Hennigan, C. J., Miracolo, M. A., Robinson, A. L., and Pandis, S. N.: Cloud condensation nuclei activity of fresh primary and aged biomass burning aerosol, Atmos. Chem. Phys., 12, 7285–7293, doi:10.5194/acp-12-7285-2012, 2012.

Ervens, B., Feingold, G., and Kreidenweis, S.: Influence of water-soluble organic carbon on cloud drop number concentration., J. Geophys. Res., 110, D18211, doi:10.1029/2004JD005634, 2005.

Feingold, G.: Modeling of the first indirect effect: Analysis of measurement requirements, Geophys. Res. Lett., 30, 1997, doi:10.1029/2003GL017967, 2003.

Gasparini, R., Collins, D. R., Andrews, E., Sheridan, P. J., Ogren, J. A., and Hudson, J. G.: Coupling aerosol size distributions and size-resolved hygroscopicity to predict humidity-dependent optical properties and cloud condensation nuclei spectra., J. Geophys. Res., 111, D05S13, doi:10.1029/2005JD006092, 2006.

Gunthe, S. S., King, S. M., Rose, D., Chen, Q., Roldin, P., Farmer, D. K., Jimenez, J. L., Artaxo, P., Andreae, M. O., Martin, S. T., and Pöschl, U.: Cloud condensation nuclei in pristine tropical rainforest air of Amazonia: size-resolved measurements and modeling of atmospheric aerosol composition and CCN activity, Atmos. Chem. Phys., 9, 7551–7575, doi:10.5194/acp-9-7551-2009, 2009.

Hartz, K. E. H., Tischuk, J. E., Chan, M. N., Chan, C. K., Donahue, N. M., and Pandis, S. N.: Cloud condensation nuclei activation of

limited solubility organic aerosol, Atmos. Environ., 40, 605–617, 2006.

Hudson, J.: Variability of the relationship between particle size and cloud-nucleating ability, Geophys. Res. Lett., 34, L08801, doi:10.1029/2006GL028850, 2007.

IPCC: Climate change 2013: Scientific basis, Fifth assessment of the Inter-governmental Panel on Climate Change, Cambridge Univ. Press, New York, 2013.

Jimenez, J. L., Canagaratna, M. R., Donahue, N. M., Prevot, A. S. H., Zhang, Q., Kroll, J. H., DeCarlo, P. F., Allan, J. D., Coe, H., Ng, N. L., Aiken, A. C., Docherty, K. S., Ulbrich, I. M., Grieshop, A. P., Robinson, A. L., Duplissy, J., Smith, J. D., Wilson, K. R., Lanz, V. A., Hueglin, C., Sun, Y. L., Tian, J., Laaksonen, A., Raatikainen, T., Rautiainen, J., Vaattovaara, P., Ehn, M., Kulmala, M., Tomlinson, J. M., Collins, D. R., Cubison, M. J., Dunlea, E. J., Huffman, J. A., Onasch, T. B., Alfarra, M. R., Williams, P. I., Bower, K., Kondo, Y., Schneider, J., Drewnick, F., Borrmann, S., Weimer, S., Demerjian, K., Salcedo, D., Cottrell, L., Griffin, R., Takami, A., Miyoshi, T., Hatakeyama, S., Shimono, A., Sun, J. Y., Zhang, Y. M., Dzepina, K., Kimmel, J. R., Sueper, D., Jayne, J. T., Herndon, S. C., Trimborn, A. M., Williams, L. R., Wood, E. C., Middlebrook, A. M., Kolb, C. E., Baltensperger, U., and Worsnop, D. R.: Evolution of Organic Aerosols in the Atmosphere, Science, 326, 1525–1529, 2009.

Köhler, H.: The nucleus in and growth of hygroscopic droplets, Trans. Faraday Soc., 32, 1152–1161, doi:10.1039/TF9363201152, 1936.

Kreidenweis, S. M., Petters, M. D., and DeMott, P. J.: Single-parameter estimates of aerosol water content, Environ. Res. Lett., 3, 035002 doi:10.1088/1748-9326/3/3/035002, 2008.

Kuwata, M., Kondo, Y., Mochida, M., Takegawa, N., and Kawamura, K.: Dependence of CCN activity of less volatile particles on the amount of coating observed in Tokyo, J. Geophys. Res., 112, D11207, doi:10.1029/2006JD007758, 2007.

Lance, S., Medina, J., Smith, J., and Nenes, A.: Mapping the operation of the DMT continuous flow CCN counter, Aerosol Sci. Technol., 40 , 242–254, 2006.

Lathem, T.L., and Nenes, A.: Water vapor depletion in the DMT Continuous Flow CCN Chamber: effects on supersaturation and droplet growth, Aeros. Sci. Tech., 45, 604–615, doi:10.1080/02786826.2010.551146, 2011.

Lathem, T. L., Beyersdorf, A. J., Thornhill, K. L., Winstead, E. L., Cubison, M. J., Hecobian, A., Jimenez, J. L., Weber, R. J., Anderson, B. E., and Nenes, A.: Analysis of CCN activity of Arctic aerosol and Canadian biomass burning during summer 2008, Atmos. Chem. Phys., 13, 2735–2756, doi:10.5194/acp-13-2735-2013, 2013.

Lau, K. M., Ramahathan, V., Wu, G., Li, Z., Tsay, S. C., Hsu, C., Sikka, R., Holben, B., Lu,D., Tartari, G., Chin, M., Koudelova, P., Chen, H., Ma, Y., Huang, J., Taniguchi, K., and Zhang, R.: The joint aerosol monsoon experiment: A new challenge for monsoon climate research, Bull. Am. Meteorol. Soc., 89, 369–383, doi:10.1175/BAMS-89-3-369, 2008.

Lee, S. H., Murphy, D. M., Thomson, D. S., and Middlebrook, A. M.: Nitrate and oxidized organic ions in single particle mass spectra during the 1999 Atlanta Supersite Project, J. Geophys. Res., 108, 8417, doi:10.1029/2001JD001455, 2003.

Lee, Y. S., Collins, D. R., Li, R. J., Bowman, K. P., and Feingold, G.: Expected impact of an aged biomass burning aerosol on cloud condensation nuclei and cloud droplet concentrations, J. Geophys. Res., 111, D22204, doi:10.1029/2005JD006464, 2006.

Leng, C., Cheng, T., Chen, J., Zhang, R., Tao, J., Huang, G., Zha, S., Zhang, M., Fang, W., Li, X., and Li, L.: Measurements of surface cloud condensation nuclei and aerosol activity in downtown Shanghai, Atmos. Environ., 69, 354–361, 2013.

Li, Z., Chen, H., Cribb, M., Dickerson, R. E., Holben, B., Li, C., Lu, D., Luo, Y., Maring, H., Shi, G., Tsay, S.-C., Wang, P., Wang, Y., Xia, X., Zheng, Y., Yuan, T., and Zhao, F.: Preface to special section on East Asian Studies of Tropospheric Aerosols: An International Regional Experiment (EASTAIRE), J. Geophys. Res., 112, D22S00, doi:10.1029/2007JD008853, 2007a.

Li, Z., Xia, X., Cribb, M., Mi, W., Holben, B., Wang, P., Chen, H., Tsay, S-C., Eck, T. F., Zhao, F., Dutton, E. G., and Dickerson, R. E.: Aerosol optical properties and their radiative effects in northern China, J. Geophys. Res., 112, D22S01, doi:10.1029/2006JD007382, 2007b.

Li, Z., Li, C., Chen, H., Tsay, S.-C., Holben, B., Huang, J., Li, B., Maring, H., Qian, Y., Shi, G., Xia, X., Yin, Y., Zheng, Y., and Zhuang, G.: East Asian Studies of Tropospheric Aerosols and Impact on Regional Climate (EAST-AIRC): An overview, J. Geophys. Res., 116, D00K34, doi:10.1029/2010JD015257, 2011.

Liu, J., Zheng, Y., Li, Z., and Cribb, M.: Analysis of cloud condensation nuclei properties at a polluted site in southeastern China during the AMF-China Campaign, J. Geophys. Res., 116, D00K35, doi:10.1029/2011JD016395, 2011.

Ma, Y., Brooks, S. D., Vidaurre, G., Khalizov, A. F., and Wang, L.: Rapid modification of cloud-nucleating ability of aerosols by biogenic emissions, Geophys. Res. Lett. 40, 6293–6297, doi:10.1002/2013GL057895, 2013.

Mei, F., Setyan, A., Zhang, Q., and Wang, J.: CCN activity of organic aerosols observed downwind of urban emissions during CARES, Atmos. Chem. Phys., 13, 12155–12169, doi:10.5194/acp-13-12155-2013, 2013.

Mikhailov, E., Vlasenko, S., Martin, S. T., Koop, T., and Pöschl, U.: Amorphous and crystalline aerosol particles interacting with water vapor: conceptual framework and experimental evidence for restructuring, phase transitions and kinetic limitations, Atmos. Chem. Phys., 9, 9491–9522, doi:10.5194/acp-9-9491-2009, 2009.

Mircea, M., Facchini, M. C., Decesari, S., Cavalli, F., Emblico, L., Fuzzi, S., Vestin, A., Rissler, J., Swietlicki, E., Frank, G., Andreae, M. O., Maenhaut, W., Rudich, Y., and Artaxo, P.: Importance of the organic aerosol fraction for modeling aerosol hygroscopic growth and activation: a case study in the Amazon Basin, Atmos. Chem. Phys., 5, 3111–3126, doi:10.5194/acp-5-3111-2005, 2005.

Niedermeier, D., Wex, H., Voigtländer, J., Stratmann, F., Brüggemann, E., Kiselev, A., Henk, H., and Heintzenberg, J.: LACIS-measurements and parameterization of sea-salt particle hygroscopic growth and activation, Atmos. Chem. Phys., 8, 579–590, doi:10.5194/acp-8-579-2008, 2008.

Ng, N. L., Herndon, S. C., Trimborn, A., Canagaratna, M. R., Croteau, P. L., Onasch, T. B., Sueper, D.,Worsnop, D. R., Zhang, Q., Sun, Y. L., and Jayne, J. T.: An Aerosol Chemical Speciation Monitor (ACSM) for Routine Monitoring of the Composition and Mass Concentrations of Ambient Aerosol, Aerosol Sci. Tech., 45, 770–784, 2011.

Padró, L. T., Tkacik, D., Lathem, T. L., Hennigan, C. J., Sullivan, A. P., Weber, R. J., Huey, L. G., and Nenes, A.: Investigation of cloud condensation nuclei properties and droplet growth kinetics of the water-soluble aerosol fraction in Mexico City, J. Geophys. Res., 115, D09204, doi:10.1029/2009JD013195, 2010.

Paramonov, M., Aalto, P. P., Asmi, A., Prisle, N., Kerminen, V.-M., Kulmala, M., and Petäjä, T.: The analysis of size-segregated cloud condensation nuclei counter (CCNC) data and its implications for cloud droplet activation, Atmos. Chem. Phys., 13, 10285–10301, doi:10.5194/acp-13-10285-2013, 2013.

Petters, M. D. and Kreidenweis, S. M.: A single parameter representation of hygroscopic growth and cloud condensation nucleus activity, Atmos. Chem. Phys., 7, 1961–1971, doi:10.5194/acp-7-1961-2007, 2007.

Petters, M. D., Carrico, C. M., Kreidenweis, S. M., Prenni, A. J., DeMott, P. J., Collett, J. L., and Moosmüller, H.: Cloud condensation nucleation activity of biomass burning aerosol, J. Geophys. Res., 114, D22205, doi:10.1029/2009JD012353, 2009.

Quinn, P. K., Bates, T. S., Coffman, D. J., and Covert, D. S.: Influence of particle size and chemistry on the cloud nucleating properties of aerosols, Atmos. Chem. Phys., 8, 1029–1042, doi:10.5194/acp-8-1029-2008, 2008.

Raymond, T. M. and Pandis, S. N.: Cloud activation of single component organic aerosol particles, J. Geophys. Res., 107, 4787, doi:10.1029/2002JD002159, 2002.

Rissler, J., Swietlicki, E., Zhou, J., Roberts, G., Andreae, M. O., Gatti, L. V., and Artaxo, P.: Physical properties of the submicrometer aerosol over the Amazon rain forest during the wet-to-dry season transition – comparison of modeled and measured CCN concentrations, Atmos. Chem. Phys., 4, 2119–2143, doi:10.5194/acp-4-2119-2004, 2004.

Roberts, G. C., Artaxo, P., Zhou, J. C., Swietlicki, E., and Andreae, M. O.: Sensitivity of CCN spectra on chemical and physical properties of aerosol: A case study from the Amazon Basin, J. Geophys. Res., 107, 8070, doi:10.1029/2001JD000583, 2002.

Rose, D., Gunthe, S. S., Mikhailov, E., Frank, G. P., Dusek, U., Andreae, M. O., and Pöschl, U.: Calibration and measurement uncertainties of a continuous-flow cloud condensation nuclei counter (DMT-CCNC): CCN activation of ammonium sulfate and sodium chloride aerosol particles in theory and experiment, Atmos. Chem. Phys., 8, 1153–1179, doi:10.5194/acp-8-1153-2008, 2008.

Rose, D., Nowak, A., Achtert, P., Wiedensohler, A., Hu, M., Shao, M., Zhang, Y., Andreae, M. O., and Pöschl, U.: Cloud condensation nuclei in polluted air and biomass burning smoke near the mega-city Guangzhou, China – Part 1: Size-resolved measurements and implications for the modeling of aerosol particle hygroscopicity and CCN activity, Atmos. Chem. Phys., 10, 3365–3383, doi:10.5194/acp-10-3365-2010, 2010.

Rose, D., Gunthe, S. S., Su, H., Garland, R. M., Yang, H., Berghof, M., Cheng, Y. F., Wehner, B., Achtert, P., Nowak, A., Wiedensohler, A., Takegawa, N., Kondo, Y., Hu, M., Zhang, Y., Andreae, M. O., and Pöschl, U.: Cloud condensation nuclei in polluted air and biomass burning smoke near the mega-city Guangzhou, China – Part 2: Size-resolved aerosol chemical composition, diurnal cycles, and externally mixed weakly CCN-active soot particles, Atmos. Chem. Phys., 11, 2817–2836, doi:10.5194/acp-11-2817-2011, 2011.

Rosenfeld, D., Dai, J., Yu, X., Yao, Z., Xu, X., Yang, X., and Du, C.: Inverse relations between amounts of air pollution and orographic precipitation, Science, 315, 1396–1398, doi:10.1126/science.1137949, 2007.

Salcedo, D., Onasch, T. B., Dzepina, K., Canagaratna, M. R., Zhang, Q., Huffman, J. A., DeCarlo, P. F., Jayne, J. T., Mortimer, P., Worsnop, D. R., Kolb, C. E., Johnson, K. S., Zuberi, B., Marr, L. C., Volkamer, R., Molina, L. T., Molina, M. J., Cardenas, B., Bernabé, R. M., Márquez, C., Gaffney, J. S., Marley, N. A., Laskin, A., Shutthanandan, V., Xie, Y., Brune, W., Lesher, R., Shirley, T., and Jimenez, J. L.: Characterization of ambient aerosols in Mexico City during the MCMA-2003 campaign with Aerosol Mass Spectrometry: results from the CENICA Supersite, Atmos. Chem. Phys., 6, 925–946, doi:10.5194/acp-6-925-2006, 2006.

Sotiropoulou, R. E. P., Nenes, A., Adams, P. J., and Seinfeld, J. H.: Cloud condensation nuclei prediction error from application of Köohler theory: Importance for the aerosol indirect effect, J. Geophys. Res., 112, D12202, doi:10.1029/2006JD007834, 2007.

Streets, D. G., Yu, C., Wu, Y., Chin, M., Zhao, Z., Hayasaka, T., and Shi, G.: Aerosol trends over China, 1980–2000, Atmos. Res., 88, 174–182, doi:10.1016/j.atmosres.2007.10.016, 2008.

Stroud, C. A., Nenes, A., Jimenez, J. L., DeCarlo, P., Huffman, J. A., Bruintjes, R., Nemitz, E., Delia, A. E., Toohey, D. W., Guenther, A. B., and Nandi, S.: Cloud Activating Properties of Aerosol Observed during CELTIC, J. Atmos. Sci., 64, 441–459, 2007.

Sun, Y., Wang, Z., Dong, H., Yang, T., Li, J., Pan, X., Chen, P., and Jayne, J. T.: Characterization of summer organic and inorganic aerosols in Beijing, China with an Aerosol Chemical Speciation Monitor, Atmos. Environ., 51, 250–259, doi:10.1016/j.atmosenv.2012.01.013, 2012.

Takegawa, N., Miyakawa, T., Kawamura, K., and Kondo, Y.: Contribution of selected di-carboxylic and omega-oxocarboxylic acids in ambient aerosol to the m/z 44 signal of an aerodyne aerosol mass spectrometer, Aerosol Sci. Technol., 41, 418–437, doi:10.1080/02786820701203215, 2007.

Turpin, B. J. and Lim, H. J.: Species contributions to $PM_{2.5}$ mass concentrations: Revisiting common assumptions for estimating organic mass, Aerosol Sci. Tech., 35, 602–610, 2001.

Twomey, S.: Pollution and planetary albedo, Atmos. Environ., 8, 1251–1256, 1974.

VanReken, T. M., Rissman, T. A., Roberts, G. C., Varutbangkul, V., Jonsson, H. H., Flagan, R. C., and Seinfeld, J. H.: Toward aerosol/cloud condensation nuclei (CCN) closure during CRYSTAL-FACE, J. Geophys. Res., 108, 4633, doi:10.1029/2003JD003582, 2003.

VanReken, T. M., Ng, N. L., Flagan, R. C., and Seinfeld, J. H.: Cloud condensation nucleus activation properties of biogenic secondary organic aerosol, J. Geophys. Res., 110, D07206, doi:10.1029/2004JD005465, 2005.

Varutbangkul, V., Brechtel, F. J., Bahreini, R., Ng, N. L., Keywood, M. D., Kroll, J. H., Flagan, R. C., Seinfeld, J. H., Lee, A., and Goldstein, A. H.: Hygroscopicity of secondary organic aerosols formed by oxidation of cycloalkenes, monoterpenes, sesquiterpenes, and related compounds, Atmos. Chem. Phys., 6, 2367–2388, doi:10.5194/acp-6-2367-2006, 2006.

Whitby, K., T.: The physical characteristics of sulfur aerosols, Atmos. Environ., 12, 135–159, 1967, Online publication date: 1 January 1978, 1978.

Xia, X., Li, Z., Holben, B., Wang, P., Eck, T., Chen, H., Cribb, M., and Zhao, Y.: Aerosol optical properties and radiative effects in the Yangtze Delta region of China, J. Geophys. Res., 112, D22S12, doi:10.1029/2007JD008859, 2007.

Xin, J., Wang, Y., Li, Z., Wang, P., Hao, W., Nordgren, B. L., Wang, S., Liu, G., Wang, L., Wen, T., Sun, Y., and Hu, B.: AOD and Angstrom exponent of aerosols observed by the Chinese Sun Hazemeter Network from August 2004 to September 2005, J. Geophys. Res., 112, D05203, doi:10.1029/2006JD007075, 2007.

Xu, Q.: Abrupt change of the mid-summer climate in central east China by the influence of atmospheric pollution, Atmos. Environ., 35, 5029–5040, doi:10.1016/S1352-2310(01)00315-6, 2001.

Yue, D. L., Hu, M., Zhang, R. J., Wu, Z. J., Su, H., Wang, Z. B., Peng, J. F., He, L.Y., Huang, X. F., Gong, Y. G., and Wiedensohler, A.: Potential contribution of new particle formation to cloud condensation nuclei in Beijing, Atmos. Environ., 45, 6070–6077, 2011.

Yum, S. S., Roberts, G., Kim, J. H., Song, K., and Kim, D.: Submicron aerosol size distributions and cloud condensation nuclei concentrations measured at Gosan, Korea, during the Atmospheric Brown Clouds–East Asian Regional Experiment 2005, J. Geophys. Res., 112, D22S32, doi:10.1029/2006JD008212, 2007.

Zhang, Q., Stanier, C. O., Canagaratna, M. C., Jayne, J. T., Worsnop, D. R., Pandis, S. N., and Jimenez, J. L.: Insights into the Chemistry of New Particle Formation and Growth Events in Pittsburgh Based on Aerosol Mass Spectrometry, Environ. Sci. Technol., 38, 4797–4809, 2004.

Zhang, Q., Meng, J., Quan, J., Gao, Y., Zhao, D., Chen, P., and He, H.: Impact of aerosol composition on cloud condensation nuclei activity, Atmos. Chem. Phys., 12, 3783–3790, doi:10.5194/acp-12-3783-2012, 2012.

Zhang, R., Khalizov, A. F., Pagels, J., Zhang, D., Xue, H., and McMurry, P. H.: Variability in morphology, hygroscopic and optical properties of soot aerosols during internal mixing in the atmosphere, Proc. Natl. Acad. Sci. USA, 105, 10291–10296, 2008.